Cite this: *Soft Matter*, 2011, **7**, 10737

www.rsc.org/softmatter

PAPER

Stimulus responsive self-assembly of Gemini Amphiphilic Pseudopeptides†

Jenifer Rubio,[a] Ignacio Alfonso,*[b] M. Isabel Burguete[a] and Santiago V. Luis*[a]

Received 27th July 2011, Accepted 30th August 2011
DOI: 10.1039/c1sm06435e

Amphiphilic amino acid derived compounds are very interesting for the design of building blocks able to self-assemble into highly ordered nanostructures, in a hierarchical and controlled fashion. With this aim, the modular synthesis and the full characterization of simple Gemini Amphiphilic Pseudopeptides (GAPs) have been carried out. These compounds were designed to establish intermolecular interactions in a hierarchical way to finally render supramolecular assemblies into well-ordered nanostructures, such as fibers, tubes, tapes or spherical vesicles. Different structural variables have been implemented, such as the amino acid side chain, the length of the central spacer and the nature of the hydrophobic tails. Besides, the effect of the environment was systematically checked, by performing the studies in solvents of different polarities (chloroform, methanol or aqueous methanol) and at different pHs (neutral, basic and acidic). The non-covalent self-assembling abilities and the structural features of the GAPs have been studied in the solid (SEM, TEM and FT-IR) and in the solution states (NMR, UV, CD, FT-IR and fluorescence spectroscopy). Moreover, the connection between the solution and the solid states has been established by monitoring the slow evaporation of the solvent by ATR FT-IR. This study has allowed the establishment of a relationship between the chemical structures of the GAPs and their abilities to form nanostructures. In some optimal cases (especially for the valine derivatives with medium-length spacers and two decyloxybenzyl hydrophobic tails), they behaved as stimulus responsive self-assembling nano-structures, which form amorphous materials from non-polar solvents, nano-fibers from polar environments at neutral or basic pH and vesicles when become protonated at acidic pH values. A reasonable structural model to explain the experimental observations can be proposed through the combination of the results from the different techniques.

Introduction

The controlled self-assembly of small molecules into a well-defined structure in the nanometric scale has become a very active research field during the last decade.[1–3] The formation of the corresponding nanostructure is dictated by the combination of intermolecular non-covalent interactions,[4–9] which work cooperatively to define the shape and dimensions of the final nano-object.[10–12] This methodology has been called the bottom-up approach to nanotechnology; it is a biomimetic strategy and represents the natural approximation for chemists.[4,6,13–20] Peptides and peptide-like molecules are among the most interesting families of building blocks for this bottom-up construction.[7,21–31] Amino acids are molecules with a high functional density and a large potential for structural diversity, which allows the implementation of many non-covalent interactions with a minimum number of elements in the design.[32–34] Accordingly, the self-assembly of many peptide-like compounds into nanostructures has been described in the literature, with promising applications in biomedicine and for the fabrication of new materials.[33,35–45] On the other hand, amphiphilic molecules are also interesting species in the self-assembling field, since they are able to display a dual behavior depending on the environment.[46–50] Especially, they have been used for preparing nano-objects in highly polar environments, with interesting potential to be used in biological applications, as they mimic the structure of compounds essential for the generation of important bioassemblies.[51–53]

The most interesting topic within this field should be the possibility to make the self-assembling system able to respond to a simple external stimulus, thus triggering the formation of a given nanostructure, or for obtaining different nano-objects from the same building blocks under controlled conditions.[54–59] To this aim, different stimuli have been used like polarity of the medium, pH, enzymatic reactions, dilution or the presence of chemicals and reducing agents.[60–69]

[a]*Departamento de Química Inorgánica y Orgánica, Universitat Jaume I, Avenida Sos Baynat, s/n, Castellón, Spain. E-mail: luiss@qio.uji.es; Fax: +34 964728214; Tel: +34 964728239*

[b]*Departamento de Química Biológica y Modelización Molecular, Instituto de Química Avanzada de Cataluña (IQAC-CSIC), Jordi Girona 18-26, Barcelona, Spain. E-mail: ignacio.alfonso@iqac.csic.es; Fax: +34 932045904; Tel: +34 934006100*

† Electronic supplementary information (ESI) available: Full spectra characterization of all the described compounds and additional experimental data. See DOI: 10.1039/c1sm06435e

Here we report on the design, synthesis and characterization of different Gemini Amphiphilic Pseudopeptides (thereafter named GAPs)[70] able to self-assemble into nanostructures displaying different shapes like fibers, tubes, tapes or vesicles. More interestingly, the self-assembling process can be controlled through the polarity of the environment and, for some specific examples, can be switched between fibers and vesicles by simple variation of the pH.

Results and discussion

Design and synthesis of the GAPs building blocks

The GAPs considered in this work were designed to display different intermolecular polar and non-polar interactions. Their main structural characteristics are depicted in Fig. 1.

They possess two amino acid moieties connected through their acid ends by a flexible spacer, and two hydrophobic tails at both amino termini, rendering an overall C_2 symmetry. This design will allow the modular implementation of several functional groups with the potential of establishing different interactions (H-bond, dipole–dipole, π-stacking, hydrophobic or van der Waals contacts, *etc.*). Moreover, the GAPs have also two secondary amino nitrogens, which display the corresponding acid–base properties, and the possibility of the systems to respond to pH changes.

The synthesis of the proposed GAPs has been carried out following a simple procedure as depicted in Scheme 1. First of all, the corresponding C_2 symmetrical bis(amidoamines) were prepared using previously reported procedures.[71] After that, the *N*,*N*′-dialkylated compounds were prepared by a reductive amination reaction with different aldehydes.[72–74] The selection of both the solvent and the reducing agent was not trivial for this step, and, after an optimization study, we found that the combination of chloroform and the borane–pyridine complex led to the best yields and selectivity towards the dialkylated derivative (Table 1).[70,75,76] The results mainly depend on the structure of the starting aldehyde, leading to higher yields in the case of aromatic aldehydes. Although the yields with the aliphatic aldehydes were moderate to low, the complete selectivity towards the dialkylated compound made this procedure of synthetic interest. Besides, considering the low solubility of the final compounds in these cases, we believe that the lower yields observed can be associated to the problems found during their isolation. In some cases, the corresponding monoalkylated derivative was obtained as a by-product (yields in brackets in Table 1), being readily separated from the GAPs by flash chromatography. The reaction can be performed with pseudopeptides having aliphatic (Me, iPr, iBu) or aromatic (Bn) side chains, and with different spacers between amino acid moieties. Some

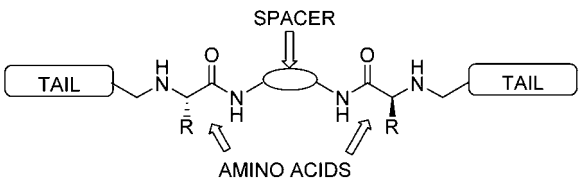

Fig. 1 General structure of the GAPs.

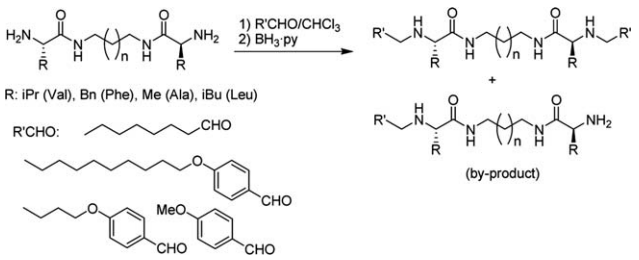

Scheme 1 Synthesis of the GAPs by a reductive amination reaction.

compounds bearing shorter tails (entries 14 and 15) were also prepared as references for the self-assembling studies (see below).

For a clearer discussion, we will use a systematic code for the naming of the compounds (Table 1) as follows: **A*N*Xxx_a(tail)** where ***N*** means the total number of carbon atoms of the central spacer (and thus, $N = n + 2$), **Xxx** is the three letter code for the corresponding amino acid, and the tail is named as **a8** for octyl, **a1obenz** for methoxybenzyl, **a4obenz** for butyloxybenzyl and **a10obenz** for decyloxybenzyl. Thus, for instance, A4Val_a10obenz would be the GAP derived from valine with a butylenic spacer and two decyloxybenzyl tails.

Ultrastructure in the solid state

In order to study the ability of the GAPs to self-assemble into supramolecular nano-structures in the solid state we performed Scanning Electron Microscopy (SEM) experiments for samples (*ca.* 2 mg mL^{-1}) slowly evaporated onto aluminium surfaces. Also, for selected examples, Transmission Electron Microscopy (TEM) images were taken, rendering similar morphologies to those observed by SEM, although with slightly smaller sizes, probably due to the differences in sample preparation for both techniques. The samples were grown from solvents of different polarities such as $CHCl_3$, MeOH or aqueous (33% v/v) MeOH in order to study the effect of the environment in the aggregation behavior. Besides, the protonation of the secondary amino groups of the GAPs was also studied by preparing the samples in aqueous methanol containing a slight excess of acid. The observations are summarized in Table 2 and selected images are shown in Fig. 2–4, the rest being provided as ESI (Fig. S1–S4†). Different nano-structures were observed ranging from fibrils, fibers, tapes, tubes or even spheres, depending on the structure of the GAPs and on the solvent used for growing the samples.[77–79]

Several general trends can be concluded from this study. First of all, the GAPs show low tendency to self-organize in chloroform, since only a few of them form nanostructures when evaporated from this medium. Mainly the compounds bearing aliphatic tails and ethylene (A2Val_a8, entry 9) or propylene (A3Val_a8, entry 10) spacers self-aggregate in chloroform yielding hollow tubes or tapes (Fig. 2), respectively. The saddle structural changes rendering important supramolecular differences suggested that the morphology of the nanostructures is dictated by the conformation of the central spacer, which leads to completely different disposition and shape of the overall GAP.

However, upon increasing the polarity of the solvent, we observed the formation of nanostructures for many of the GAPs, most of them appearing as fibers with different sizes and widths

Table 1 Synthesis of the GAPs

	Spacer (*n*)	Aaa (R)	Tail (CH_2R')	Compound	Yield[a]
1	$(CH_2)_2$ (0)	Val (iPr)	$CH_2C_6H_4OC_{10}H_{21}$	A2Val_a10obenz	63 [5][b]
2	$(CH_2)_3$ (1)	Val (iPr)	$CH_2C_6H_4OC_{10}H_{21}$	A3Val_a10obenz	68 [15][b]
3	$(CH_2)_4$ (2)	Val (iPr)	$CH_2C_6H_4OC_{10}H_{21}$	A4Val_a10obenz	66 [19][b]
4	$(CH_2)_5$ (3)	Val (iPr)	$CH_2C_6H_4OC_{10}H_{21}$	A5Val_a10obenz	38 [19][b]
5	$(CH_2)_6$ (4)	Val (iPr)	$CH_2C_6H_4OC_{10}H_{21}$	A6Val_a10obenz	67 [9][b]
6	$(CH_2)_2$ (0)	Phe (Bn)	$CH_2C_6H_4OC_{10}H_{21}$	A2Phe_a10obenz	66 [21][b]
7	$(CH_2)_3$ (1)	Phe (Bn)	$CH_2C_6H_4OC_{10}H_{21}$	A3Phe_a10obenz	61 [19][b]
8	$(CH_2)_4$ (2)	Phe (Bn)	$CH_2C_6H_4OC_{10}H_{21}$	A4Phe_a10obenz	74 [23][b]
9	$(CH_2)_2$ (0)	Val (iPr)	C_8H_{17}	A2Val_a8	26
10	$(CH_2)_3$ (1)	Val (iPr)	C_8H_{17}	A3Val_a8	21
11	$(CH_2)_4$ (2)	Val (iPr)	C_8H_{17}	A4Val_a8	32
12	$(CH_2)_4$ (2)	Ala (Me)	$CH_2C_6H_4OC_{10}H_{21}$	A4Ala_a10obenz	48 [26][b]
13	$(CH_2)_4$ (2)	Leu (iBu)	$CH_2C_6H_4OC_{10}H_{21}$	A4Leu_a10obenz	63 [12][b]
14	$(CH_2)_4$ (2)	Val (iPr)	$CH_2C_6H_4OCH_3$	A4Val_a1obenz	77
15	$(CH_2)_4$ (2)	Val (iPr)	$CH_2C_6H_4OC_4H_9$	A4Val_a4obenz	70 [12][b]

[a] Isolated yields (%) for the one-pot two-steps reductive amination reaction. [b] Numbers in brackets correspond to the monoalkylated by-product.

(Fig. 3). Among all the measured compounds in MeOH, only three of them were unable to form nanostructures (entries 1, 2 and 6). It is worth mentioning that those observations correspond to GAPs having the smaller spacers: A2 (entries 1 and 6) or A3 (entry 2). Very interestingly, the compounds with benzyloxyalkyl tails having short alkyl groups (entries 14 and 15 for Me and Bu alkyl groups, respectively) also showed the formation of fibers when evaporated from MeOH. This suggests that the central pseudopeptidic moiety must be playing a major role in the aggregation process, maybe through the establishment of intermolecular H-bonding interactions. This proposal is also in line with the formation of fibers due to the high directionality of H-bonds, which would induce the growing of the nanostructures in a preferred direction. The further increase of the polarity by using 33% (v/v) of water in the MeOH did not significantly change the aggregation abilities (Fig. 3d). In this mixture of solvents, we also tested the effect of the pH, by performing the experiments in neutral, basic and acidic media. No important changes were observed from neutral to basic media. However, the situation in the presence of acid is completely different. The fiber-like nanostructures were destroyed in most of the studied examples upon protonation, except for the derivatives with completely aliphatic tails (entries 9–11 in Table 2). Very surprisingly, for some specific cases having decyloxybenzyl tails and Val or Ala amino acids, the formation of spheres of micrometric size was observed (entries 2, 3, 4 and 12 and Fig. 4). Besides, the formation of microspheres is observed for compounds having an intermediate number of atoms in the

Table 2 Self-assembling properties of the GAPs

	Compound	$CHCl_3$[a]	MeOH[a]	MeOH (aq)[a]	MeOH/H^+[a]	CMC[c]
1	A2Val_a10obenz	Fibrils	No	No	No	85
2	A3Val_a10obenz	No	No	No	Vesicles	16
3	A4Val_a10obenz	No	Fibers	Fibers	Vesicles	13
4	A5Val_a10obenz	No	Fibers	Fibers	Vesicles	20
5	A6Val_a10obenz	No	Fibers	Fibers	No	63
6	A2Phe_a10obenz	No	No	No	No	>100
7	A3Phe_a10obenz	No	Fibers	Fibers	No	>100
8	A4Phe_a10obenz	No	Fibers	Fibers	No	48
9	A2Val_a8	Tubes	Fibers	Fibers	Fibers	n.m[d]
10	A3Val_a8	Tapes	Tapes	Tapes	Non-hom.[b]	n.m[d]
11	A4Val_a8	No	Fibers	Fibers	Fibers	n.m[d]
12	A4Ala_a10obenz	Fibrils	Fibers	Fibers	Vesicles	16
13	A4Leu_a10obenz	No	Fibrils	Fibers	No	62
14	A4Val_a1obenz	No	Fibers	Fibers	No	>100
15	A4Val_a4obenz	No	Fibers	Fibers	No	>100

[a] Nanostructures observed by electron microscopy in samples grown from different solvents. [b] Non-hom.: SEM images showed non-homogeneous formation of both fibrils and spheres, accompanied with amorphous material. [c] CMC (μM): critical micellar concentration in water at pH 2.7 (AcOH/AcONa buffer) determined by fluorescence spectroscopy using pyrene as a probe. [d] n.m.: not measured.

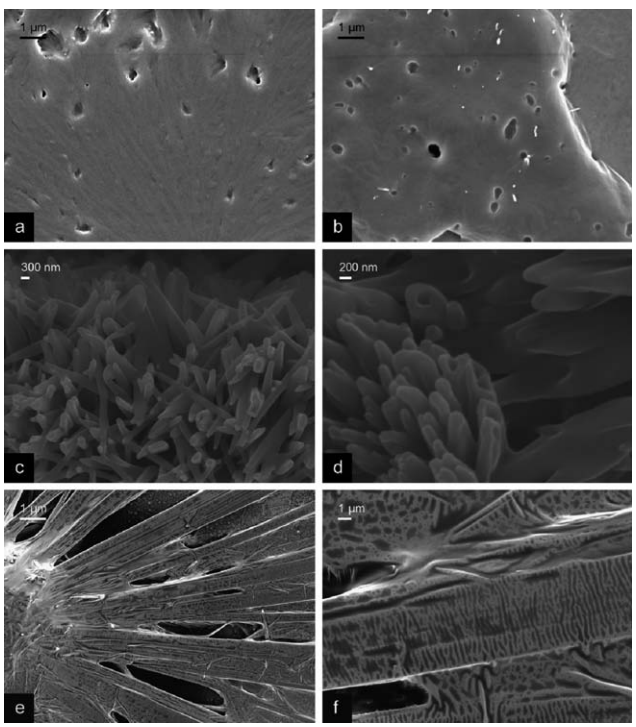

Fig. 2 SEM micrographs of (a) A4Val_a1obenz, (b) A4Phe_a10obenz, (c and d) A2Val_a8 and (e and f) A3Val_a8 grown from $CHCl_3$ solutions. The corresponding scale bars are shown for every picture.

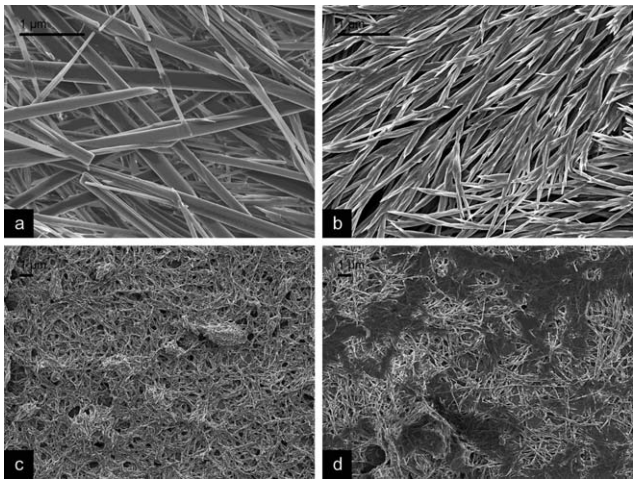

Fig. 3 Selected SEM micrographs for (a) A4Val_a1obenz, (b) A2Val_a8, (c) A4Leu_a10obenz and (d) A6Val_a10obenz grown from MeOH (a–c) or 2 : 1 MeOH : H_2O (d) solutions. The corresponding scale bars are shown for every picture.

central spacer (from three to five, n = 1–3). Either shorter or longer spacers produced amorphous materials in acidic medium. Therefore, there is a strong correlation between the chemical structure of the GAP and its ability to self-assemble into spheres. Thus, for instance, the compound having the butylenic spacer (A4Val_a10obenz, with a length in the middle of those forming spheres) can be considered as a stimulus dependent self-assembling GAP, since it forms amorphous material in $CHCl_3$, fibers in MeOH or aqueous MeOH at neutral and basic pH, while providing spheres in acidic medium (Fig. 4). These morphologies have been studied by both SEM and TEM techniques, which suggested that the spheres are hollow and, therefore, can be classified as vesicles attending to their dimensions and the molecular size of the building blocks (Fig. 4d and f). Within the same central pseudopeptidic frame, the nature of the tails is highly important for the formation of these vesicles.

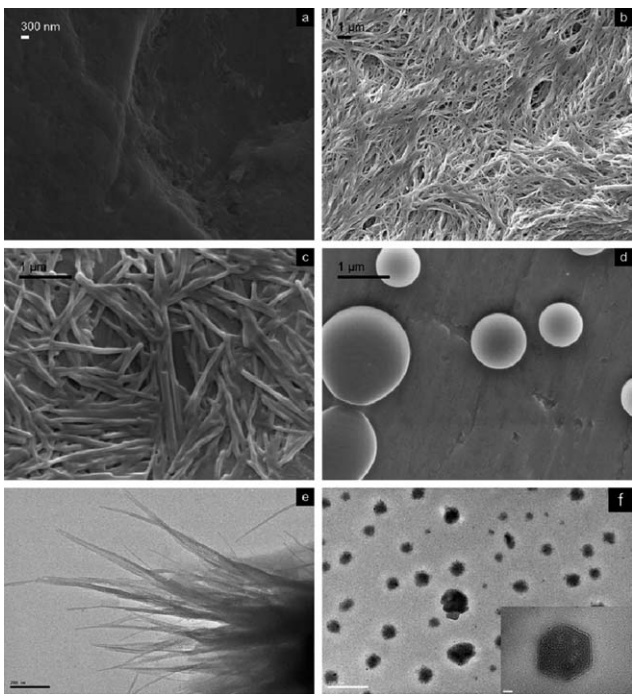

Fig. 4 Effect of the environment on the self-assembling of A4Val_a10obenz. SEM micrographs of A4Val_a10obenz grown from (a) $CHCl_3$, (b) MeOH, (c) 2 : 1 MeOH : H_2O and (d) 2 : 1 MeOH : H_2O + HCl. TEM images of A4Val_a10obenz grown from (e) MeOH and (f) 2 : 1 MeOH : H_2O + HCl.

The decyloxybenzyl groups seem to be an essential feature in this regard since the compounds having shorter alkyloxybenzyl (A4Val_a1obenz and A4Val_a4obenz) or fully aliphatic residues (A2Val_a8, A3Val_a8 and A4Val_a8) at the amino nitrogens, either failed to form any nanostructure (entries 14 and 15 in Table 2), or led to a fibrilar morphology (entries 9 and 11) or to a non-homogeneous mixture (entry 10). Overall, we have found that with a delicate tune of the molecular architecture and the environment conditions, a control over the self-assembling in the solid state can be carried out. Thus, transition from amorphous materials to fibers or vesicles can be observed in several cases, especially in Val derivatives with decyloxybenzyl tails and a spacer of a medium length (n = 1–3).

Solution structure of the GAPs

With the aim of getting deeper information on the conformational and structural behavior of the GAPs in a pre-aggregated state, before the formation of the self-assembled nanostructures, we have carried out a systematic study of the compounds in solution, by using a broad variety of spectroscopic techniques. Thus, we have performed NMR, UV, CD and fluorescence studies of selected examples under different conditions. Finally, we have also studied the transition from the diluted solution to the solid state by monitoring the evaporation of the solvent by ATR FT-IR spectroscopy.

NMR spectroscopy. The ^{1}H NMR spectra of some selected GAPs were studied in different solvents ($CDCl_3$ and CD_3OD), in the absence and in the presence of acid (DCl in D_2O), at different temperatures and at two overall concentrations (1 mM and 20 mM). Considering the results obtained in the solid state, we selected the compounds displaying a more distinct self-assembling behavior in different media.

Therefore, the Val derivatives with the decyloxybenzyl tails and bearing spacers of different lengths were selected for this systematic NMR study (Fig. S5–S15 and Tables S1–S3†). First of all, a very small effect was observed when changing the overall concentration of the GAPs from 1 mM to 20 mM, which suggested that no significant aggregation was present over that concentration range. Thus, the NMR study should mainly correspond to fully solvated pre-aggregated species. Anyway, knowledge of the conformational behavior and the inter/intramolecular interactions is of interest to rationalize the self-assembling observations in the solid state. Clear differences were observed on the NMR spectra when changing the polarity of the medium. Thus, for instance, we studied the ^{1}H NMR spectra in different conditions for A4Val_a10obenz (Fig. 5 and ESI†). The chemical shift (>7.00 ppm) and temperature dependence ($\Delta\delta$NH/$\Delta T = -3.5$ ppb K^{-1}) of the amide NH protons signal in $CDCl_3$ suggested the presence of partially H-bonded amide groups. The

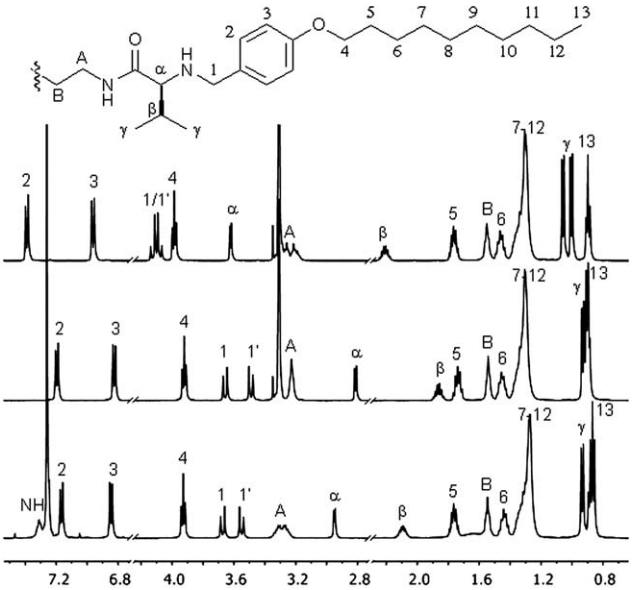

Fig. 5 ^{1}H NMR (500 MHz, 303 K) spectra of A4Val_a10obenz in $CDCl_3$ (down), CD_3OD (middle) and CD_3OD + DCl (up). Assignations of the signals are shown following the arbitrary lettering of the chemical substructure.

high chemical shift values of protons at α and β positions are also in line with this proposal. Besides, the methylene vicinal to the amide group (A in Fig. 5) showed chemical non-equivalence [$\Delta\delta(H_{A/A'}) = 0.052$ ppm at 294 K], which was decreased upon heating [$\Delta\delta(H_{A/A'}) = 0.038$ ppm at 323 K]. All these observations suggested that the pseudopeptidic moiety is intramolecularly H-bonded in a relatively rigid conformation. However, when acquiring the ^{1}H NMR spectrum in methanol, the signals corresponding to the protons from the pseudopeptidic moiety (α, β, γ and A) moved up-field, while those from the hydrophobic tails did not significantly change. More importantly, the hydrogen atoms of the methylenes in the A position lost their chemical non-equivalence, appearing as a broad triplet. These observations were consistent with the breaking of the intramolecularly H-bonded pseudopeptidic structure, leading to an unfolded and more flexible conformation in solution. Protonation of A4Val_a10obenz in CD_3OD also affected the NMR spectrum. Thus, the presence of a positive charge at the amino nitrogen produced large downfield shifts at the positions 1, α, β and γ. Besides, the deshielding of protons at 2, 3 and 4 suggested that the anisole substructure was highly polarized upon nitrogen protonation. On the other hand, the signals from the hydrophobic tail suffered a slight up-field shift (0.01–0.02 ppm). Surprisingly, the anisochrony of the protons at position A [$\Delta\delta(H_{A/A'}) = 0.043$ ppm] again suggested a restricted mobility of the butylenic spacer for the protonated form of A4Val_a10obenz, and a different chemical environment for both faces of the spacer.

We observed similar trends for the other derivatives (see ESI† for details), suggesting that the central pseudopeptidic spacer behaved in a similar way. Thus, we can conclude that the different behavior in the transition from the fibers to the vesicles is an effect of the structural relationship between this moiety and the hydrophobic tails (see below).

Molecular electronic spectroscopy (UV-CD). Those selected GAPs were also studied by electronic spectroscopy (UV) and circular dichroism (CD) in solution. The large absorbance of chloroform at 220–230 nm precluded the accurate study of the systems in this solvent. Thus, we focused on the effect of the protonation in MeOH solution, bearing in mind that the changes in the self-assembling behavior were also accompanied by a change in the flexibility of the GAPs in solution, as suggested by the ^{1}H NMR spectra, in the presence and in the absence of acid. Moreover, the UV-CD spectra were acquired at different concentrations (0.012–0.583 mM) showing a perfect linear dependence of the absorbance *versus* the concentration, which also suggested the absence of aggregated species at this concentration range. Different structural parameters in the GAPs were varied, like the length of the central spacer, the amino acid side chain and the hydrophobic tails.

The length of the central spacer had an important impact on the UV-CD spectra. The UV spectra in MeOH at neutral pH showed two characteristic bands: one very intense at 226–230 nm (π–π* transition) and another less intense at 273–276 nm (*n*–π* transition). The corresponding UV-CD spectra for compounds A*N*Val_a10obenz (with $N = 2$–6) are superposed in Fig. 6A. The molar extinction coefficient is dependent on the length of the spacer, being highest with the butylenic one ($n = 2$, A4Val_a10obenz). Regarding the CD spectra in MeOH, all the compounds showed a weak negative Cotton effect at 230 nm. Interestingly, if we represent the Δε of the CD spectra *versus* the spacer (Fig. 6B), once again the most intense CD signal was obtained for the medium-sized spacers. This observation correlates with the fact that these were the GAPs showing a higher propensity to form fibers in SEM.

The addition of acid produced important changes in the UV-CD spectra, which were significantly different for each compound (Fig. 6C). Thus, the variation of the UV absorbance strongly depended on the length of the spacer (Fig. 6D), showing a strong hypochromic effect of both maxima for $n = 2$ (A4Val_a10obenz). Concomitantly, an almost complete disappearance of the CD signal was observed upon protonation. The reduction of the CD signal due to the transition from fibers to vesicles has been previously reported[61,80,81] but, in our case, the CD measurements were performed in a pre-aggregated state.

Thus, we ascribed the almost silent CD spectra to the presence of a mixture of conformations in solution with a complementary geometrical disposition of the chromophores, finally rendering a null effect on the CD spectra (see below). Another interesting observation, after the protonation, is the appearance of a band at lower energy at 330 nm, which can be assigned to a charge transfer (CT) band (Fig. 6E). This CT can be produced by the interaction between the anisole chromophore on one side of the GAP and the ammonium group on the other side, in a folded conformation. According to this hypothesis, this CT band is maximum for the shortest spacer (close proximity between groups), but does not uniformly decay with the separation between the interacting groups. Once again, we observed a discontinuity for the butylenic spacer showing a slightly more effective CT than the propylenic one (Fig. 6F) and suggesting a more efficient folding of the GAP with this spacer.

Other structural parameters were also studied by UV-CD spectroscopy, by keeping constant the butylenic spacer ($N = 4$).

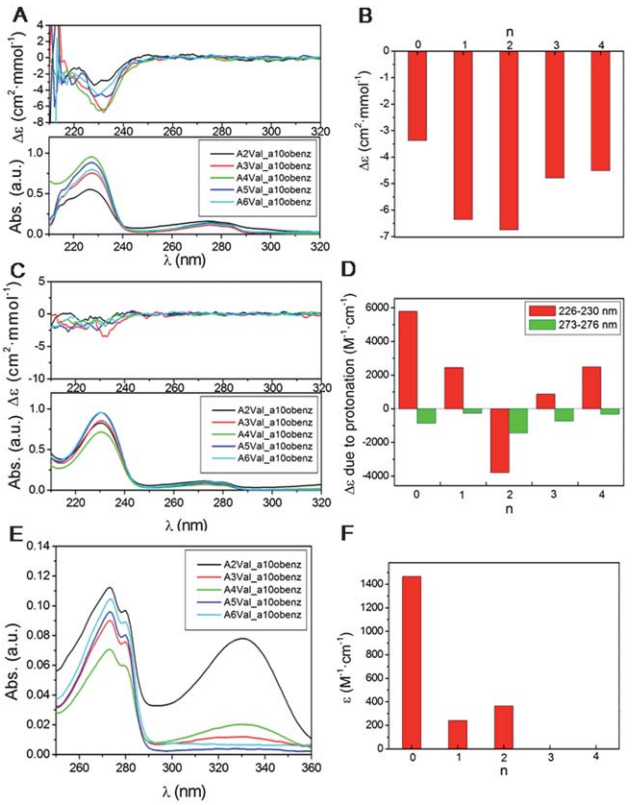

Fig. 6 (A) UV-CD spectra of A*N*Val_a10obenz ($N = 2$–6) in MeOH. (B) Plot of the $\Delta\varepsilon$ of the CD spectra of A*N*Val_a10obenz ($N = 2$–6) in MeOH *versus* n ($n = N-2$). (C) UV-CD spectra of A*N*Val_a10obenz ($N = 2$–6) in MeOH in the presence of acid. (D) Plot of the variation of UV extinction coefficients at the corresponding maxima due to protonation *versus* n. (E) Zoomed UV spectra of A*N*Val_a10obenz ($N = 2$–6) in MeOH in the long wavelength region. (F) Plot of the variation of UV extinction coefficient for the CT band.

For instance, in order to understand the role of the aliphatic tail attached to the benzyloxy moiety, we measured the UV-CD spectra of the GAP bearing a short methyl group (A4Val_a1obenz). Interestingly, for this compound, there was practically no change of the UV and CD spectra upon protonation (Fig. 7A). Thus, the conformational changes associated to protonation (observable by UV and CD) require the presence of the long hydrophobic chain in the tails.

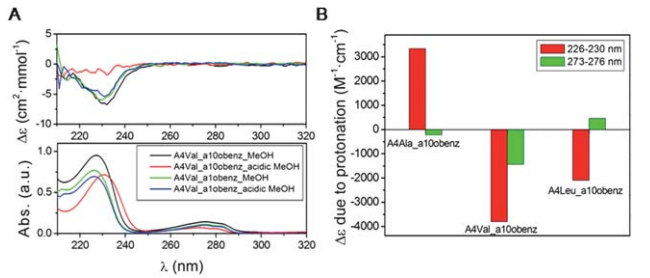

Fig. 7 (A) UV-CD spectra of A4Val_a10obenz and A4Val_a1obenz in MeOH in the absence and in the presence of acid. (B) Plot of the variation of UV extinction coefficients at the corresponding maxima due to protonation for several amino acid side chains.

Considering the observations in the solid state, this fact must also be related to the ability of the systems to produce the transition from fibers to vesicles upon protonation. On the other hand, the effect of the amino acid side chain was also evaluated by UV (Fig. 7B). The most dramatic decrease of the UV absorbance upon protonation occurred with Val derivatives, when compared to Ala or Leu. This is in agreement with the ability for the formation of vesicles (previous section and below) and must be related to the presence of a substituent in the β-carbon of the amino acid moiety.[61–63]

Overall, taking into account all the UV-CD measurements, some general conclusion can be drawn. First of all, the polarity of the media and the protonation in the GAPs produced important changes in the UV and CD spectra. Considering the protonation, those changes are more dramatic for the compounds bearing a butylenic spacer. These changes seem to be related to a folding of the chromophores and require the presence of the long hydrophobic chain on the tails. Among all the amino acid side chains tested, the Val derivative showed the most marked differences in the protonation process, which is in agreement with the ability shown to form vesicles.

Fluorescence spectroscopy. Taking into account the formation of vesicles by the GAPs in acidic polar environments, we decided to study their aggregation in water at acidic pH in a more quantitative way. To this aim, we have measured the critical micellar concentration (CMC) by fluorescence spectroscopy using pyrene as the fluorescent probe.[82,83] This method takes advantage of the sensitivity of the pyrene emission spectrum to the polarity of the medium. All the measurements were performed in aqueous acetic/acetate buffer at pH 2.7. The CMC was obtained by plotting the ratio between the first and the third band of the emission spectrum of pyrene (I_1/I_3) *versus* the overall concentration of the GAP (in log scale). The CMC was

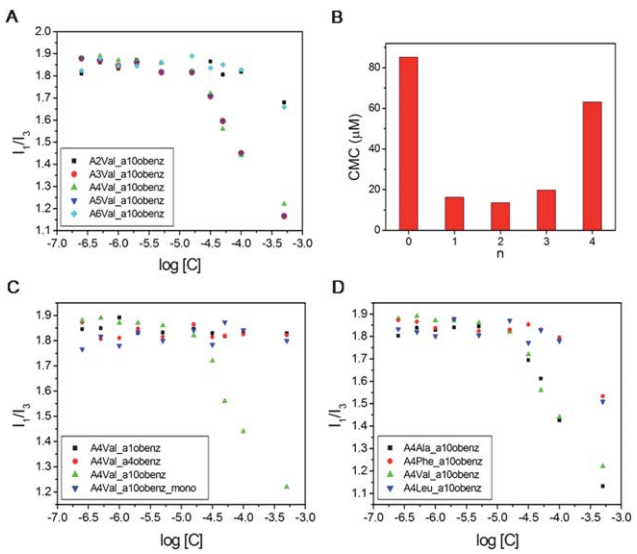

Fig. 8 (A) Plots of I_1/I_3 fluorescence intensity of pyrene *versus* log C of the GAPs for A*N*Val_a10obenz ($N = 2$–6) to study the effect of the spacer on the CMC. (B) Plot of the CMC values as a function of the spacer length (n). (C) Effect of the hydrophobic tail on the I_1/I_3 plot. (D) Effect of the amino acid side chain on the I_1/I_3 plot.

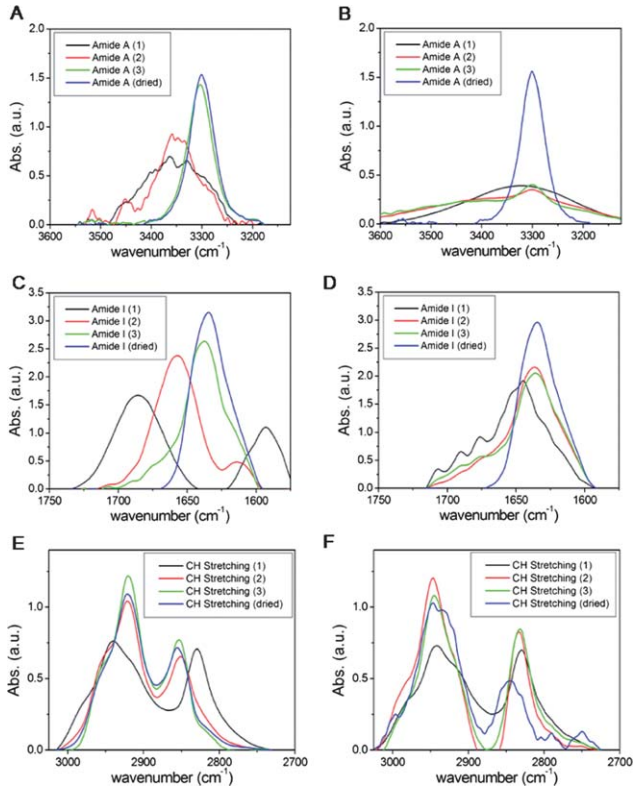

Fig. 9 Selected regions of several ATR FT-IR spectra of A4Val_a10obenz: (A) amide A in $CHCl_3$, (B) amide A in MeOH, (C) amide I in $CHCl_3$, (D) amide I in MeOH, (E) C–H stretching in MeOH, and (F) C–H stretching in MeOH with acid.

calculated by extrapolation of the slopes for the two straight lines observed (Fig. 8).

The values for the CMC are given in Table 2 showing that the lower is the CMC, the more efficient is the assembly in water. The results obtained are in good agreement with those observed by UV-CD experiments, regarding the tendency to self-assemble into vesicles. For instance, the spacers with an intermediate length are more efficient as observed in Fig. 8A, the butylenic one being the best in this regard (Fig. 8B, entries 1–5 in Table 2). The effect of the hydrophobic tails was also studied (Fig. 8C) by measuring the corresponding methyl (A4Val_a1obenz, black symbols) and butyl (A4Val_a4obenz, red symbols) GAPs which did not produce changes in the fluorescence of pyrene up to 1 mM concentrations. We also studied the corresponding mono-alkylated compound (A4Val_a10obenz_mono, Fig. 8C, blue symbols) obtained as a by-product in the synthesis of A4Val_a10obenz. The results supported that two hydrophonic tails are needed for the vesicle formation. Finally, the effect of the side chain was also studied, rendering the Val derivative as the most efficient pseudopeptide for the assembly in acidic water (Table 2 and Fig. 8D). These data are in agreement with the results obtained in solid state by microscopy and in solution by other spectroscopic techniques, and rendered the compound A4Val_a10obenz as the most interesting GAP regarding efficiency and diversity in the formation of nanostructures upon the action of external stimuli, such as solvent polarity or pH.

Attenuated total reflectance Fourier transform infrared (ATR FT-IR) spectroscopy. The connection between the solution behavior (pre-assembled state) and the solid state nanostructures can be carried out by ATR FT-IR spectroscopy, which is very suitable for the study of the self-assembling process itself.[84] First of all, the vibrational modes of some characteristic functional groups are very sensitive to the environment and to the inter/intramolecular interactions. Besides, FT-IR can be performed with practically all the states of matter and thus, results in solution and in solid state can be directly compared.

Accordingly, we decided to monitor the self-assembling process from the pre-aggregated state in solution to the final solid state nanostructures. For this study, we selected the compound A4Val_a10obenz, which displayed the most interesting behavior regarding its stimulus dependent self-assembly. For this, 20 mM solutions of this GAP (the most concentrated solutions studied by NMR, showing no aggregation) were placed onto the ATR sampler holder, and the corresponding FT-IR spectra were acquired at different time intervals during the slow evaporation of the solvent (concentration of the sample) until obtaining the dry nanostructure (Fig. 9). With this procedure, the variation of some representative IR bands can be monitored while the self-assembly of the GAP is taking place onto the ATR sampler holder. This study was performed in chloroform, MeOH and

Table 3 ATR FT-IR data (cm^{-1}) of A4Val_a10obenz in different media

Solv.	Samp.[a]	Amide A[b]	C–H stretch[b]	Amide I[b]	Amide II[b]
$CHCl_3$	1	3364 (b)	2945, 2866 (b)	1686 (b)	1527 (b)
	2	3347 (b)	2928, 2859 (b)	1657 (b)	1515 (b)
	3	3303 (m)	2922, 2856 (m)	1637 (m)	1548, 1515(m)
	Dry	3301 (m-s)	2922, 2856 (m)	1634 (m-s)	1546, 1509(m)
MeOH	1	3345 (b)	2943, 2830 (b)	1645 (b)	1549, 1515 (b)
	2	3300 (b-m)	2920, 2851 (m)	1636 (m)	1549, 1515(m)
	3	3300 (b-m)	2920, 2853 (s)	1636 (m)	1549, 1515(m)
	Dry	3300 (s)	2929, 2858 (s)	1634 (s)	1549, 1515(m)
$MeOH/H^+$	1	Overlapped	2947, 2830 (b)	1669 (b)	1451 (b)
	2	Overlapped	2947, 2833 (m)	1661 (b)	1451 (b)
	3	Overlapped	2947, 2833 (s)	1661 (b)	1451 (b)
	Dry	Overlapped	2947, 2833 (s)	1661 (b)	1451 (b)

[a] Samples '1–3' corresponded to acquisition at increasing concentrations obtained by the evaporation of the solvent while 'dry' states for the solid sample. [b] The letters in parenthesis describe the shape of the band (b: broad, m: medium, s: sharp).

MeOH with a slight excess of acid (Fig. 9 and Table 3), since this compound showed very different self-assembling behavior from those environments. In general, the evaporation of the solvent produced important changes in the bands assigned to the amide N–H stretching (amide A at 3300–3400 cm^{-1}), the aliphatic C–H stretching (2800–3000 cm^{-1}, two bands corresponding to symmetric and asymmetric stretching), the C=O stretching (1600–1700 cm^{-1}, amide I) and the on-plane N–H bending (1500–1570 cm^{-1}, amide II). In chloroform (Fig. 9A and C), all the bands suffered an important sharpening while the solvent evaporates, suggesting a more rigid and symmetric structure in the solid state. The amide A (Fig. 9A) appears as a broad band centered at 3364 cm^{-1} in solution and evolves towards a sharper peak at 3301 cm^{-1}, which suggested the establishing of intermolecular H-bonding interactions upon evaporation. This is also in agreement with the evolution of the amide I (Fig. 9C) and amide II (ESI†) bands, which experienced a red-shift and a sharpening (Table 3). The growing of the fibers from methanol is characterized by a very important sharpening and a red shift of the signals assigned to amide A and amide I bands (Fig. 9B and D, Table 3), suggesting the formation of well defined C=O···H–N intermolecular H-bonds. The final values of the wavenumbers for these bands in the dried fibers (Table 3) are in agreement with a β-stack conformation of the pseudopeptidic moiety.[85] On the other hand, the values of the C–H stretching frequencies suggested a liquid crystal-like phase of the hydrophobic tails (Table 3).[86] When comparing the IR data in chloroform and in methanol (compare Fig. 9A *vs.* B and C *vs.* D), we can observe that the spectral motif of the dried sample is already present in solution for methanol but not for chloroform. This becomes more evident when the deconvolution of the bands is carried out (ESI†). Thus, for instance, the relative proportion of the H-bound N–H band is higher in MeOH solution (previous to dryness) than in $CHCl_3$. Thus, we concluded that in MeOH at concentrated solutions, the compound is pre-aggregated through intermolecular H-bonding and hydrophobic contacts.

The IR spectra acquired from acidic MeOH also provided important information. First of all, the amide N–H band could not be analyzed because it was overlapped with the ammonium N–H band (ESI†). The carbonyl stretching showed a very broad band centered at 1661 cm^{-1} during all the evaporation process, which suggested the presence of different carbonyls in the aggregated species and discarded the participation of this group in the interactions for the assembling. The most important feature of the spectra acquired in acidic medium was the sharp band observed for the symmetric C–H stretching, at a lower value (2847 cm^{-1}) than in neutral MeOH (2858 cm^{-1}), as shown in Fig. 9E and F for the neutral and acidic MeOH solutions, respectively. This observation suggests a more ordered disposition of the aliphatic tails in acidic medium and points to the importance of the hydrophobic interactions between them for the formation of the vesicles.

Model for the interaction

Considering all the studies performed in the solid state and in solution, we also aimed to propose a reasonable model to explain the observed behavior. First of all, we must stress that there is a close relationship between the chemical structure of the GAPs and their ability to self-assemble. Besides, for the most interesting examples, the compounds are able to aggregate in a different fashion depending on the polarity of the medium or the presence of an acid (Fig. 10). Thus, in $CHCl_3$, the ^1H NMR data showed that the pseudopeptides tend to fold by intramolecular H-bonding interactions. On the other hand, the hydrophobic tails are fully solvated in this solvent. This precludes the ordered organization of the systems through intermolecular contacts in a pre-aggregated state in solution (as observed by ATR FT-IR) and, for most of the examples, amorphous materials were observed in the solid state (SEM). In MeOH, the H-bonding interactions with the solvent unfold the GAPs leading to a more flexible extended conformation (as suggested by NMR). This structure is now able to organize in solution in a pre-aggregated state through H-bonding and van der Waals contacts (as observed by ATR FT-IR). The main interaction is the H-bonding in a β-stack conformation (FT-IR), which is highly directional and finally renders the formation of fiber-like nanostructures. This is supported by the data obtained with the A4Val_a1obenz derivative, which is able to yield fibers in spite of lacking the long hydrophobic tails.

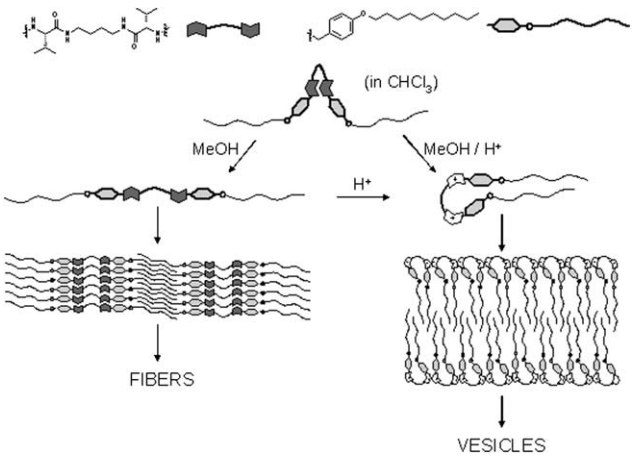

Fig. 10 Schematic representation of the self-assembling behaviour of the GAPs in different conditions, represented for A4Val_a10benz.

The protonation of the GAPs in aqueous MeOH changed the self-assembling behavior for most of the examples. Most interestingly, the compounds having very specific structural features were able to form vesicles (SEM and TEM). A deep spectroscopic study (NMR and UV) suggested that the GAPs also present a rigid conformation in acidic media, with a folded structure (NMR and UV) where the hydrophobic interactions play a major role in the stability of the folding (UV and CD) and in the formation of the vesicles. Besides, there is a strict relationship between the vesicle formation ability and the length of the central spacer. The fully protonated GAPs would set the ammonium groups as distant as possible to minimize electrostatic interactions and thus, an extended conformation should be expected for the aliphatic central spacer. In this conformation, a very interesting trend can be obtained when comparing the distance between the ammonium group and the oxygen of the benzyloxy moiety *versus* the distance between the ammonium and the center of the spacer (Fig. 11A). These distances nicely match for the butylenic spacer (difference 0.02 Å) and gradually

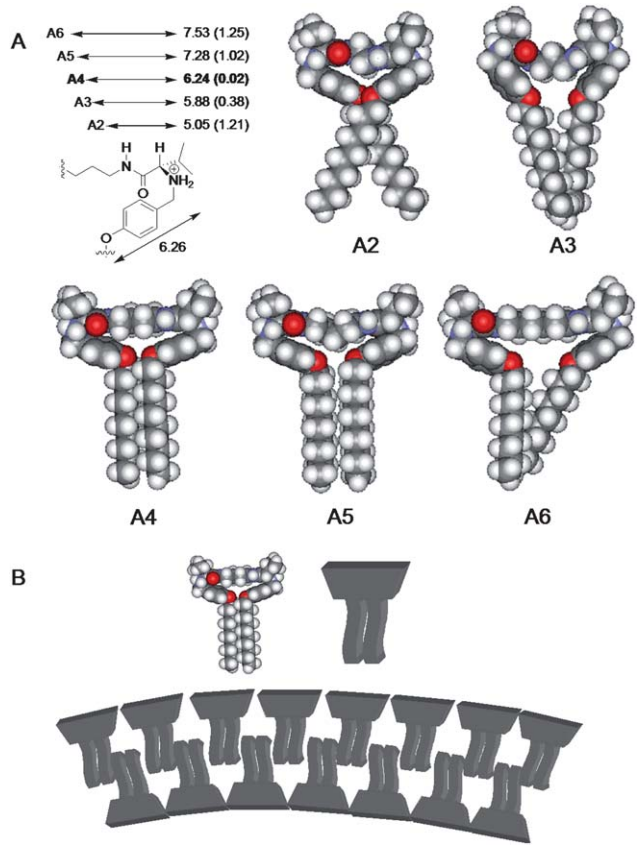

Fig. 11 (A) Structural relationships (distances in Å) and molecular models for A*N*Val_a10obenz ($N = 2$–6). (B) Schematic representation of the proposal for the formation of bilayers.

become unfit as far as the spacer is either longer or shorter. Molecular mechanics calculations showed the possibility of stable energy minima with a conformation setting the aromatic rings folded over the pseudopeptidic moiety.

Besides, for the best matched distances (A3, A4 and A5), this conformation favors the van der Waals contacts between the long hydrophobic tails, being the best structural complementarity for A4. This observation is in agreement with the ability to form vesicles, which was optimal for the A4Val_a10obenz compound. Actually, the cationic gemini surfactant-like disposition in a T-shaped molecular structure would explain the assembly in a curved bilayer finally rendering the formation of vesicles, as experimentally observed (Fig. 11B). The van der Waals contacts between the tails are much less efficient for the

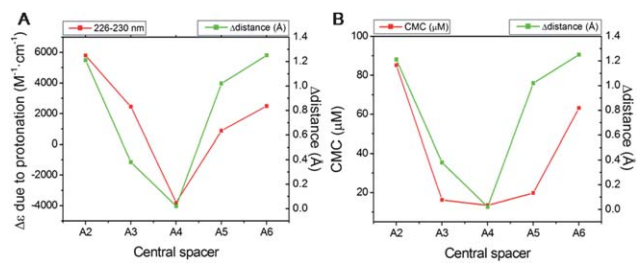

Fig. 12 Correlation between structural and spectroscopic parameters.

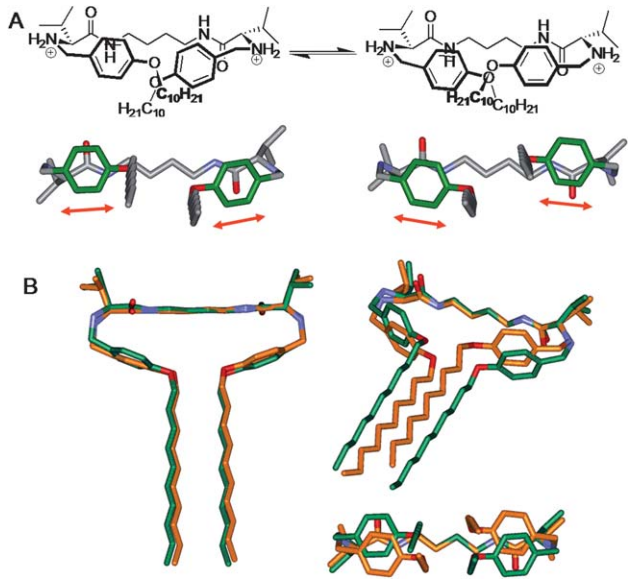

Fig. 13 (A) Proposed equilibrium between the two conformers of protonated A4Val_a10obenz, with the chromophores highlighted. (B) Superimposed structures in several views. For clarity, the hydrogen atoms have been omitted and the carbon atoms have been represented in a different color for each minimum.

shortest (A2) and the longest (A6) spacer, which nicely explain our experimental observations. Actually, if we plot the discrepancy in the previously commented distances and some experimental data (UV changes due to protonation or CMC measured by fluorescence) *versus* the length of the spacer, a very good correlation between them is observed (Fig. 12).

This model is also in good agreement with other spectroscopic observations in solution state. For instance, the large anisochrony in the ^{1}H NMR signals of the methylenes of the spacer directly attached to the N (protons A in Fig. 5) can be explained by the large anisotropy effect of the anisole ring placed at one face of the spacer (like in our model). Additionally, this geometry would correlate with the red-shift of the symmetric C–H stretching bands in the IR spectra, since the efficient contacts between the tails would rigidify their conformation. This disposition would also favor an electronic communication between the anisole ring and the pseudopeptidic moiety (Fig. S28† for the frontier orbitals on a simplified model) which could explain the changes observed in the UV spectra upon protonation. Regarding the silent CD signal, for protonated A4Val_a10obenz, we found two energetically very close conformations with a complementary disposition of the chromophores, but retaining the same molecular shape and interactions (Fig. 13). Considering the dipole moment changes associated to the transitions, these structures would produce mirror CD signals and thus, we concluded that the co-existence of both geometries might produce low or null CD spectra.

Conclusions

The syntheses and full characterization (including ultrastructure characterization) of new Gemini Amphiphilic Pseudopeptides (GAPs) have been carried out. The formation of a large variety

of nanostructures was observed in the solid state, rendering fibers, tubes, tapes or spheres. The structural parameters and environmental effects have been systematically varied in order to get reasonable structure/nanostructure relationships, based on the intermolecular non-covalent interactions between the corresponding building blocks. For some specific structural features, a stimulus dependent self-assembling behavior was observed, which produced amorphous materials in chloroform, fibers in polar solvents and vesicles upon protonation. This behavior was especially efficient for the GAPs derived from Valine, with a spacer of medium length (from 3 to 5 methylenes) and bearing two decyloxybenzyl hydrophobic tails. Solution state studies using different spectroscopic techniques (NMR, UV, CD, fluorescence and ATR FT-IR) were employed to correlate the pre-aggregated species with the formation of the final nanostructures. The absence of nanostructures in non-polar medium can be related to the ability of the GAPs to establish intramolecular H-bond interactions in a partially folded conformation, and to the efficient solvation of the hydrophobic tails. In polar environments, the H-bonds with the solvent would unfold the GAPs leading to an extended conformation which self-assemble upon concentration through intermolecular H-bonding and van der Waals contacts. The main role of the H-bonds was expressed through the directionality of the aggregation into fibers. The protonation of these GAPs produced a conformational change to a new folded structure. For some specific GAPs, those species are able to self-assemble into spherical vesicles mainly due to the intermolecular hydrophobic contacts between tails, in a cationic surfactant-like mode. Thus, we have been able to rationalize our results in the formation of nanostructures on the basis of structural parameters. We envision that the understanding of the aggregation process within these simple amphiphilic amino acid derivatives will allow us to further design pseudopeptidic molecules able to form a desired nanostructure under given conditions and, more interestingly, to undergo controlled transitions between different shapes and sizes of the nano-objects.

Experimental section

General

Reagents and solvents were purchased from commercial suppliers (Adrich, Fluka or Merck) and were used without further purification. The C_2 symmetrical bis(amidoamines) were prepared as previously described.[71]

Electron microscopy

Scanning Electron Microscopy was performed either in a LEO 440I or in a JEOL 7001F microscope with a digital camera. Samples were obtained by slow evaporation of a solution of the compounds ($\sim$1 to 2 mg ml^{-1}) directly onto the sample holder, and were conventionally coated previous to the measurement. Transmission Electron Microscopy was carried out in a JEOL 2100 microscope at 120 KV. The micrographs were obtained from $\sim$1 mg ml^{-1} solutions onto a holey carbon copper grid. The samples were sonicated for 10 minutes previous to the measurement, one drop added onto the grid and collected directly without staining.

NMR spectroscopy

The NMR experiments were carried out on a Varian INOVA 500 spectrometer (500 MHz for ^{1}H and 125 MHz for ^{13}C) or on a Varian UNITY 300 (300 MHz for ^{1}H and 75 MHz for ^{13}C). Chemical shifts are reported in ppm using TMS as a reference.

Infrared spectroscopy

FT-IR spectra were acquired in a JASCO 6200 equipment having a MIRacle Single Reflection ATR Diamond/ZnSe accessory. A 20 mM sample of the corresponding pseudopeptide was prepared and seeded onto the ATR sample holder. The FT-IR spectra were sequentially collected until complete solvent evaporation. The raw IR data were processed with the JASCO spectral manager software and the deconvolution of the bands was performed with Origin software, using Gaussian-shaped ideal peaks.

UV and CD spectroscopy

Spectra were recorded with a JASCO J-810 spectropolarimeter at RT. The normalized CD spectra were obtained by transforming the molar circular dichroic absorption data ($\Delta\varepsilon$, cm^2 mmol^{-1}) using the formula: $\Delta\varepsilon = \theta/(32980Cl)$, in which θ is the measured ellipticity (in mdeg), C is the concentration (in M) and l is the path length (in cm). Molar extinction coefficients of the UV spectra were obtained by linear regression between the measured absorbance and the sample concentration.

Steady-state fluorescence spectroscopy

Steady-state fluorescence spectra were recorded in a Spex Fluorog 3–11 equipped with a 450 W xenon lamp. Fluorescence spectra were recorded in the front face mode. All the samples were measured in aerated conditions, unless otherwise stated.

Molecular modeling

All the theoretical calculations were performed with Spartan 06 software, using the MMFF level of theory for the geometry optimizations.

General procedure for the reductive amination reaction

Synthesis of A2Val_a10obenz. The corresponding pseudopeptidic bis(amidoamine) precursor (216.0 mg, 0.836 mmol) was dissolved in 5 mL of $CHCl_3$ and the solution was placed inside a flask under nitrogen atmosphere. Then, 4-decyloxybenzaldehyde (476.1 μL, 452.3 mg, 1.672 mmol) was dissolved in 5 mL of $CHCl_3$, this solution was added over the solution of the diamine and afterwards, 7 mL of $CHCl_3$ were added until a final volume of 17 mL (0.05 M final concentration each). The mixture was stirred overnight, then a large excess of $Py\cdot BH_3$ (889.0 μL, 817.9 mg, 8.36 mmol) was carefully added at 35 °C, and the mixture was allowed to react for 24 h before being hydrolyzed (conc. HCl, to acidity) and evaporated to dryness. The residue obtained was dissolved in water, basified with 1N NaOH, and extracted with $CHCl_3$. The combined organic layers were dried ($MgSO_4$) and evaporated in vacuum. The product was purified by flash chromatography on silica gel using CH_2Cl_2 as eluent, increasing slowly the polarity with MeOH and several

drops of aqueous ammonia. Yield = 63%; mp 95–104 °C; $[\alpha]_D^{25} = -27.0$ ($c = 0.01$, $CHCl_3$); IR (ATR) 3303, 2921, 2851, 1641, 1555, 1513 cm^{-1}; ^{1}H-NMR (500 MHz, $CDCl_3$) δ 0.79 (m, 18H), 0.86 (m, 24H), 1.23 (m, 4H), 1.38 (s, 2H), 1.48 (m, 4H), 1.7 (m, 2H), 2.01 (m, 2H), 2.87 (m, 4H), 3.35 (dd, 2H, $J = 5.2$, 8.1 Hz), 3.45 (dd, 2H, $J = 5.4$, 8.2 Hz), 3.61 (t, 4H, $J = 6.6$ Hz), 6.77 (d, 4H, $J = 6.77$ Hz), 7.10 (d, 4H, $J = 7.10$ Hz), 7.53 (s, 2H); ^{13}C-NMR (125 MHz, $CDCl_3$) δ 14.3, 18.0, 19.8, 22.9, 26.3, 29.5, 29.8, 29.9, 31.5, 32.1, 39.6, 53.1, 68.0, 68.3, 114.8, 129.5, 131.7, 158.7, 174.7; HRMS (ESI-TOF)$^+$ measured for $C_{46}H_{78}N_4O_4$ $(M + H)^+$: 751.6101; found 751.6102. Anal. Calcd for $C_{46}H_{78}N_4O_4 \cdot H_2O$: C, 71.93; H, 11.17; N, 6.70; found: C, 71.83; H, 10.98; N, 6.90%. A small amount of the monoalkylated by-product was also isolated: yield = 5%; mp 78–82 °C; $[\alpha]_D^{25} = -2.5$ ($c = 0.01$, $CHCl_3$); IR (ATR) 3299, 2958, 2852, 1631, 1553, 1513, 1467, 1244 cm^{-1}; ^{1}H-NMR (500 MHz, $CDCl_3$) δ 0.81 (d, 6H, $J = 6.7$ Hz), 0.87 (m, 3H), 0.95 (d, 6H, $J = 6.0$ Hz), 1.30 (m, 12H), 1.43 (m, 2H), 1.65 (m, 2H), 1.76 (td, 1H, $J = 6.6$, 13.0 Hz), 2.08 (m, 1H), 2.25 (m, 1H), 2.96 (s, 1H), 3.19 (s, 1H), 3.40 (t, 4H, $J = 12.5$ Hz), 3.55 (d, 1H, $J = 12.8$ Hz), 3.69 (d, 1H, $J = 11.4$ Hz), 3.93 (t, 2H, $J = 6.5$ Hz), 6.84 (m, 2H), 7.19 (m, 2H), 7.61 (s, 2H), 7.69 (s, 2H); ^{13}C-NMR (75 MHz, $CDCl_3$) δ 14.3, 16.4, 18.1, 19.7, 22.9, 26.3, 29.5, 29.6, 29.8, 31.0, 31.4, 32.1, 39.3, 39.8, 52.9, 60.4, 67.9, 68.3, 114.8, 129.6, 131.4, 158.8, 174.7, 175.1; HRMS (ESI-TOF)$^+$ calcd for $C_{29}H_{52}N_4O_3$ $(M + H)^+$: 505.4118; found 505.4114. Anal. Calcd for $C_{29}H_{52}N_4O_3$: C, 69.01; H, 10.38; N, 11.10; found: C, 68.85; H, 10.70; N, 11.43%.

Acknowledgements

This work was supported by the Spanish Ministry of Science and Innovation (CTQ2009-14366-C02) and UJI-Bancaixa (P1-1B-2009-59). J.R. thanks MICINN for personal financial support (FPU fellowship). The support of the SCIC of the UJI for the different instrumental techniques is acknowledged.

Notes and references

1 Y. Kim, M. F. Mayer and S. C. Zimmerman, *Angew. Chem., Int. Ed.*, 2003, **42**, 1121–1126.
2 Y. Ma, S. V. Kolotuchin and S. C. Zimmerman, *J. Am. Chem. Soc.*, 2002, **124**, 13757–13769.
3 T. Park and S. C. Zimmerman, *J. Am. Chem. Soc.*, 2006, **128**, 11582–11590.
4 G. M. Whitesides and B. Grzybowski, *Science*, 2002, **295**, 2418–2421.
5 G. M. Whitesides, J. P. Mathias and C. T. Seto, *Science*, 1991, **254**, 1312–1319.
6 J. M. Lehn, *Science*, 2002, **295**, 2400–2403.
7 S. Cavalli, F. Albericio and A. Kros, *Chem. Soc. Rev.*, 2010, **39**, 241–263.
8 D. N. Reinhoudt and M. Crego-Calama, *Science*, 2002, **295**, 2403–2407.
9 M. Surin, P. G. A. Janssen, R. Lazzaroni, P. Leclère, E. W. Meijer and A. P. H. J. Schenning, *Adv. Mater.*, 2009, **21**, 1126–1130.
10 J. M. Lehn, *Angew. Chem., Int. Ed. Engl.*, 1990, **29**, 1304–1319.
11 J. M. Lehn, *Supramolecular Chemistry, Concepts and Perspectives*, Wiley-VCH, Weinheim, 1995.
12 E. Gorrea, P. Nolis, E. Torres, E. Da Silva, D. B. Amabilino, V. Branchadell and R. M. Ortuño, *Chem.–Eur. J.*, 2011, **17**, 4588–4597.
13 V. Berl, I. Huc, R. G. Khoury, M. J. Krische and J. M. Lehn, *Nature*, 2000, **407**, 720–723.
14 R. Feynman, *Eng. Sci.*, 1960, **23**, 22–36.
15 O. Ramström, T. Bunyapaiboonsri, S. Lohmann and J. M. Lehn, *Biochim. Biophys. Acta, Gen. Subj.*, 2002, **1572**, 178–186.
16 P. Pramod, K. G. Thomas and M. V. George, *Chem.–Asian J.*, 2009, **4**, 806–823.
17 T. Nakanishi, K. Ariga, T. Michinobu, K. Yoshida, H. Takahashi, T. Teranishi, H. Möhwald and D. G. Kurth, *Small*, 2007, **3**, 2019–2023.
18 A. Petitjean, L. A. Cuccia, J.-M. Lehn, H. Nierengarten and M. Schmutz, *Angew. Chem., Int. Ed.*, 2002, **41**, 1195–1198.
19 C. A. E. Hauser and S. Zhang, *Chem. Soc. Rev.*, 2010, **39**, 2780–2790.
20 A. Aggeli, I. A. Nyrkova, M. Bell, R. Harding, L. Carrick, T. C. B. McLeish, A. N. Semenov and N. Boden, *Proc. Natl. Acad. Sci. U. S. A.*, 2001, **98**, 11857–11862.
21 J. D. Hartgerink, E. Beniash and S. I. Stupp, *Science*, 2001, **294**, 1684–1688.
22 H. Cui, M. J. Webber and S. I. Stupp, *Biopolymers*, 2010, **94**, 1–18.
23 S. I. Stupp, *Nano Lett.*, 2010, **10**, 4783–4786.
24 I. Cherny and E. Gazit, *Angew. Chem., Int. Ed.*, 2008, **47**, 4062–4069.
25 R. V. Ulijn and A. M. Smith, *Chem. Soc. Rev.*, 2008, **37**, 664–675.
26 E. Gazit, *Chem. Soc. Rev.*, 2007, **36**, 1263–1269.
27 X. Zhao and S. Zhang, *Chem. Soc. Rev.*, 2006, **35**, 1105–1110.
28 S. Zhang, *Nat. Biotechnol.*, 2003, **21**, 1171–1178.
29 L. P. Hernández-Eguía, R. J. Brea, L. Castedo, P. Ballester and J. R. Granja, *Chem.–Eur. J.*, 2011, **17**, 1220–1229.
30 M. J. Krysmann, V. Castelletto, J. E. McKendrick, L. A. Clifton, I. W. Hamley, P. J. F. Harris and S. M. King, *Langmuir*, 2008, **24**, 8158–8162.
31 N. Amdursky, M. Molotskii, E. Gazit and G. Rosenman, *J. Am. Chem. Soc.*, 2010, **132**, 15632–15636.
32 J. Berg, J. Tymoczko, L. Stryer and N. D. Clarke, *Biochemistry*, W.H. Freeman and Co., 2002.
33 I. Imaz, M. Rubio-Martínez, W. J. Saletra, D. B. Amabilino and D. Maspoch, *J. Am. Chem. Soc.*, 2009, **131**, 18222–18223.
34 R. J. Brea, C. Reiriz and J. R. Granja, *Chem. Soc. Rev.*, 2010, **39**, 1448–1456.
35 T. Muraoka, C. Y. Koh, H. Cui and S. I. Stupp, *Angew. Chem., Int. Ed.*, 2009, **48**, 5946–5949.
36 J. N. Shera and X. S. Sun, *Biomacromolecules*, 2009, **10**, 2446–2450.
37 S. Ghosh and S. Verma, *Tetrahedron*, 2008, **64**, 6202–6208.
38 K. Lu, L. Guo, A. K. Mehta, W. S. Childers, S. N. Dublin, S. Skanthakumar, V. P. Conticello, P. Thiyagarajan, R. P. Apkarian and D. G. Lynn, *Chem. Commun.*, 2007, 2729–2731.
39 L. S. Birchall, S. Roy, V. Jayawarna, M. Hughes, E. Irvine, G. T. Okorogheye, N. Saudi, E. de Santis, T. Tuttle, A. A. Edwards and R. V. Ulijn, *Chem. Sci.*, 2011, **2**, 1349–1355.
40 A. Mata, L. Hsu, R. Capito, C. Aparicio, K. Henrikson and S. I. Stupp, *Soft Matter*, 2009, **5**, 1228–1236.
41 E. Torres, J. Puigmartí-Luis, A. Pérez Del Pino, R. M. Ortuño and D. B. Amabilino, *Org. Biomol. Chem.*, 2010, **8**, 1661–1665.
42 D. B. Amabilino and J. Puigmartí-Luis, *Soft Matter*, 2010, **6**, 1605–1612.
43 R. García-Fandiño, J. R. Granja, M. D'Abramo and M. Orozco, *J. Am. Chem. Soc.*, 2009, **131**, 15678–15686.
44 C. s. Reiriz, R. J. Brea, R. o. Arranz, J. L. Carrascosa, A. Garibotti, B. Manning, J. M. Valpuesta, R. n. Eritja, L. Castedo and J. R. Granja, *J. Am. Chem. Soc.*, 2009, **131**, 11335–11337.
45 G. P. Spada, S. Lena, S. Masiero, S. Pieraccini, M. Surin and P. Samorì, *Adv. Mater.*, 2008, **20**, 2433–2438.
46 W. Cai, G. T. Wang, Y. X. Xu, X. K. Jiang and Z. T. Li, *J. Am. Chem. Soc.*, 2008, **130**, 6936–6937.
47 T. Kawasaki, M. Tokuhiro, N. Kimizuka and T. Kunitake, *J. Am. Chem. Soc.*, 2001, **123**, 6792–6800.
48 I. W. Hamley, *Soft Matter*, 2011, **7**, 4122–4138.
49 V. Castelletto and I. W. Hamley, *Biophys. Chem.*, 2009, **141**, 169–174.
50 A. Kelarakis, C. Chaibundit, M. J. Krysmann, V. Havredaki, K. Viras and I. W. Hamley, *J. Colloid Interface Sci.*, 2009, **330**, 67–72.
51 H. Cui, E. T. Pashuck, Y. S. Velichko, S. J. Weigand, A. G. Cheetham, C. J. Newcomb and S. I. Stupp, *Science*, 2010, **327**, 555–559.
52 R. J. Williams, A. M. Smith, R. Collins, N. Hodson, A. K. Das and R. V. Ulijn, *Nat. Nanotechnol.*, 2009, **4**, 19–24.
53 S. Ghosh, S. K. Singh and S. Verma, *Chem. Commun.*, 2007, 2296–2298.
54 B. S. Kim, D. J. Hong, J. Bae and M. Lee, *J. Am. Chem. Soc.*, 2005, **127**, 16333–16337.
55 N. Díaz, F.-X. Simon, M. Schmutz, M. Rawiso, G. Decher, J. Jestin and P. J. Mésini, *Angew. Chem., Int. Ed.*, 2005, **44**, 3260–3264.
56 H. J. Kim, T. Kim and M. Lee, *Acc. Chem. Res.*, 2011, **44**, 72–82.
57 T. B. Schuster, D. De Bruyn Ouboter, E. Bordignon, G. Jeschke and W. Meier, *Soft Matter*, 2010, **6**, 5596–5604.

58 P. Kumaraswamy, R. Lakshmanan, S. Sethuraman and U. M. Krishnan, *Soft Matter*, 2011, **7**, 2744–2754.
59 Y. Lin, Y. Qiao, P. Tang, Z. Li and J. Huang, *Soft Matter*, 2011, **7**, 2762–2769.
60 X. Hou, W. Guo and L. Jiang, *Chem. Soc. Rev.*, 2011, **40**, 2385–2401.
61 S. R. Diegelmann, J. M. Gorham and J. D. Tovar, *J. Am. Chem. Soc.*, 2008, **130**, 13840–13841.
62 P. P. Bose, A. K. Das, R. P. Hegde, N. Shamala and B. A. Banerjee, *Chem. Mater.*, 2007, **19**, 6150–6157.
63 Y. Song, S. R. Challa, C. J. Medforth, Y. Qiu, R. K. Watt, D. Pena, J. E. Miller, F. v. Swol and J. A. Shelnutt, *Chem. Commun.*, 2004, 1044–1045.
64 H. Matsui, *J. Phys. Chem. B*, 2000, **104**, 3385–3386.
65 H. Matsui and C. Holtman, *Nano Lett.*, 2002, **2**, 887–889.
66 J. Naskar and A. Banerjee, *Chem.–Asian J.*, 2009, **4**, 1817–1823.
67 X. Yan, Q. He, K. Wang, L. Duan, Y. Cui and J. Li, *Angew. Chem., Int. Ed.*, 2007, **46**, 2431–2434.
68 A. Ajayaghosh, R. Varghese, S. Mahesh and V. K. Praveen, *Angew. Chem., Int. Ed.*, 2006, **45**, 7729–7732.
69 S. J. Choi, W. J. Jeong, T. H. Kim and Y. B. Lim, *Soft Matter*, 2011, **7**, 1675–1677.
70 J. Rubio, I. Alfonso, M. Bru, M. I. Burguete and S. V. Luis, *Tetrahedron Lett.*, 2010, **51**, 5861–5867.
71 J. Becerril, M. Bolte, M. I. Burguete, F. Galindo, E. García-España, S. V. Luis and J. F. Miravet, *J. Am. Chem. Soc.*, 2003, **125**, 6677–6686.
72 R. N. Salvatore, C. H. Yoon and K. W. Jung, *Tetrahedron*, 2001, **57**, 7785–7811.
73 I. Alfonso, M. Bolte, M. Bru, M. Isabel Burguete and S. V. Luis, *Chem.–Eur. J.*, 2008, **14**, 8879–8891.
74 I. Alfonso, M. Bolte, M. Bru, M. I. Burguete, S. V. Luis and J. Rubio, *J. Am. Chem. Soc.*, 2008, **130**, 6137–6144.
75 F. Campbell, J. Plante, C. Carruthers, M. J. Hardie, T. J. Prior and A. J. Wilson, *Chem. Commun.*, 2007, 2240–2242.
76 F. Campbell, C. A. Kilner and A. J. Wilson, *Tetrahedron Lett.*, 2010, **51**, 1361–1363.
77 I. Alfonso, M. Bolte, M. Bru, M. I. Burguete, S. V. Luis and C. Vicent, *Org. Biomol. Chem.*, 2010, **8**, 1329–1339.
78 I. Alfonso, M. I. Burguete, F. Galindo, S. V. Luis and L. Vigara, *J. Org. Chem.*, 2007, **72**, 7947–7956.
79 I. Alfonso, M. I. Burguete and S. V. Luis, *J. Org. Chem.*, 2006, **71**, 2242–2250.
80 X. Yan, Q. He, K. Wang, L. Duan, Y. Cui and J. Li, *Angew. Chem., Int. Ed.*, 2007, **46**, 2431–2434.
81 A. Ajayaghosh, R. Varghese, S. Mahesh and V. K. Praveen, *Angew. Chem., Int. Ed.*, 2006, **45**, 7729–7732.
82 K. S. Sharma, C. Rodgers, R. M. Palepu and A. K. Rakshit, *J. Colloid Interface Sci.*, 2003, **268**, 482–488.
83 T. Yoshimura, T. Ichinokawa, M. Kaji and K. Esumi, *Colloids Surf., A*, 2006, **273**, 208–212.
84 I. Alfonso, M. Bru, M. Isabel Burguete, E. García-Verdugo and S. V. Luis, *Chem.–Eur. J.*, 2010, **16**, 1246–1255.
85 H. S. Kim, J. D. Hartgerink and M. R. Ghadiri, *J. Am. Chem. Soc.*, 1998, **120**, 4417–4424.
86 M. C. Hull, L. R. Cambrea and J. S. Hovis, *Anal. Chem.*, 2005, **77**, 6096–6099.

